Aalborg Universitet

AALBORG UNIVERSITY

Harmonic-Suppressed Dual-Resonance Decoupling Network With Near-Zero Insertion Loss for Patch Antenna Arrays

Zhang, Yiming; Lan, Tian-Yan; Zhang, Shuai; Xiao, Shao Qiu

Published in:
I E E E Transactions on Antennas and Propagation

DOI (link to publication from Publisher):
10.1109/TAP.2023.3276579

Creative Commons License
CC BY 4.0

Publication date:
2023

Document Version
Accepted author manuscript, peer reviewed version

Link to publication from Aalborg University

Citation for published version (APA):
Zhang, Y., Lan, T.-Y., Zhang, S., & Xiao, S. Q. (2023). Harmonic-Suppressed Dual-Resonance Decoupling Network With Near-Zero Insertion Loss for Patch Antenna Arrays. *I E E E Transactions on Antennas and Propagation*, *71*(8), 6959-6964. https://doi.org/10.1109/TAP.2023.3276579

General rights
Copyright and moral rights for the publications made accessible in the public portal are retained by the authors and/or other copyright owners and it is a condition of accessing publications that users recognise and abide by the legal requirements associated with these rights.

- Users may download and print one copy of any publication from the public portal for the purpose of private study or research.
- You may not further distribute the material or use it for any profit-making activity or commercial gain
- You may freely distribute the URL identifying the publication in the public portal -

Take down policy
If you believe that this document breaches copyright please contact us at vbn@aub.aau.dk providing details, and we will remove access to the work immediately and investigate your claim.

Downloaded from vbn.aau.dk on: December 05, 2025

Harmonic-Suppressed Dual-Resonance Decoupling Network With Near-Zero Insertion Loss for Patch Antenna Arrays

Yi-Ming Zhang, Tian-Yan Lan, Shuai Zhang, and Shao-Qiu Xiao

***Abstract*—To suppress the coupling among patch antenna arrays and reduce out-of-band spurious, a feeding-decoupling network with harmonic suppression is proposed. The decoupling method is achieved by generating two decoupling paths between the feeding of an antenna and the radiating patch of an adjacent antenna, through a slotline-based lowpass filter and a miniaturized coupled line coupler. Despite no decoupling operation between non-adjacent elements, the coupling among them is also reduced. The decoupling and harmonic suppression are realized by sharing the same structures, making the physical layout compact. For demonstration purposes, a design of a 1×8 patch antenna array working at 4.9 GHz, integrated with the proposed decoupling structure is developed. The results indicate that within the impedance bandwidth from 4.8 to 5.1 GHz, the coupling between both adjacent and non-adjacent elements are suppressed to less than –25 dB. Besides, spurious of up to 12 GHz is well suppressed. The in-band total efficiency of the decoupled array is higher than 80%. There is nearly no insertion loss resulting from only 50-Ω transmission lines utilized with very few discontinuities, as expected.**

***Index Terms*—Multiple input multiple output antenna, antenna decoupling, filtering antenna, harmonic suppression, beam scanning.**

I. Introduction

As one of the key technologies for 5G and future wireless communication, massive multiple input multiple output (massive MIMO) scenario, featuring remarkable performance on multi-user coverage, data rate, and exploitation of spectrum, has been studied widely in the past decade [1]-[3]. As an essential part of a massive MIMO system, the massive MIMO antenna array is directly related to the ability and stability of the communication system. Since antenna elements should be positioned at a small distance for beam scanning to avoid grating lobes, the strong mutual coupling between antenna elements is becoming a significant issue. The antenna coupling effect of massive MIMO antennas has been investigated in plenty of reports, which emphasize the importance of the decoupling of massive MIMO antennas without exception [4]-[6].

In general, antenna decoupling methods can be categorized into two aspects in terms of operation locations, i.e., operated at radiating layer [7]-[9] and the feeding layer [10]-[15]. The former ones mainly focus on generating additional decoupling paths at the radiating layer, where the radiating performance should be involved, and the profile might be increased. Different from the aspect operated at the radiating layer, the one realized at the feeding layer features a low-profile, small influence on radiation, independent from the original coupling types, and can be highly integrated with RF front ends.

Manuscript received November, 2022. This work was supported by Guangdong Basic and Applied Basic Research Foundation 2023A1515011412. (Corresponding author: Shao-Qiu Xiao)

Yi-Ming Zhang, Tian-Yan Lan, and Shao-Qiu Xiao are with the School of Electronics and Information Technology, and Guangdong Provincial Key Laboratory of Optoelectronic Information Processing Chips and Systems, Sun Yat-Sen University, Guangzhou,China. (email: zhangyim9@mail.sysu.edu.cn, lanty7@mail2.sysu.edu.cn, xiaoshq8@mail.sysu.edu.cn)

Shuai Zhang is with the Antenna, Propagation and Millimeter-wave Systems (APMS) Section, Department of Electronic Systems, Aalborg University, 9220 Aalborg, Denmark (e-mail: sz@es.aau.dk).

Color versions of one or more of the figures in this article are available online at http://ieeexplore.ieee.org

Decoupling networks for two-element arrays have been widely studied in past. As for large-scale antenna arrays, the decoupling difficulty would be increased since the leakage among both adjacent and non-adjacent elements should be involved. In [13], a decoupling network was studied for linear patch antenna arrays with a narrow decoupling bandwidth of less than 2%. To reduce the mutual coupling among $M\times N$ antenna arrays, a lattice-shaped decoupling network was given in [14], where the decoupling bandwidth features a narrow response and the decoupling between non-adjacent elements was not considered. Besides, the decoupling scheme needs additional impedance-matching networks, resulting in a degradation of total efficiency by 9.5%. In [15], an aperture-loaded decoupling network was reported. The operating bandwidth ($|S2,1| \le -25$ dB) for H-plane coupled antenna array is around 2%, and there was a tradeoff between decoupling bandwidth and insertion loss.

In addition to antenna decoupling, out-of-band suppression is also important for multi-functional wireless communication platforms involving several antenna systems. At this point, the integration of decoupling and frequency selectivity would be attractive and valuable for antenna arrays. In [16], a filtering patch antenna with a self-decoupling characteristic was provided for two-element arrays with rotationally symmetrical configurations. For large-scale patch antenna arrays, a T-shaped decoupling network was proposed and studied in [17]. An additional insertion was introduced, indicating a degradation of 13% in the total efficiency after decoupling.

In this communication, a decoupling network with harmonic suppression is proposed, by establishing two decoupling apertures between the feeding of an element and the radiating patch of an adjacent element. The novelties of this work are given as follows.

(1) Two simple decoupling structures are provided and cascaded to generate two designable decoupling resonances, leading to a wide decoupling bandwidth compared to the published decoupling networks for large-scale antenna arrays.

(2) Harmonic suppression is generated by the proposed decoupling structures. This means that the decoupling and harmonic suppression structures are highly integrated with a compact layout.

(3) No additional impedance matching network is used, and the main feeding path of the antennas is composed of several 50-Ω transmission lines, resulting in nearly no insertion loss.

(4) Non-adjacent elements are also decoupled despite no direct decoupling operation between them.

II. Decoupling Principle

Illustrated in Fig. 1 is a $1\times N$ probe-fed patch antenna array integrated with the proposed two-order decoupling networks. The center distance between adjacent elements is half-wavelength referring to the center frequency. Taking the decoupling between *Antenna N*-1 and *Antenna N* for example, the decoupling structure is an asymmetrical network, and also serves as the feeding of *Antenna N*-1, which consists of two decoupling apertures, as marked in Fig. 1(a). The first decoupling aperture is a slotline-based lowpass filter with harmonic suppression. A decoupling path could be generated between the slotline and the radiating patch of *Antenna N*. The second decoupling aperture is a coupler between a transmission line and the feeding probe of *Antenna N*. The feeding of *Antenna N*-1,

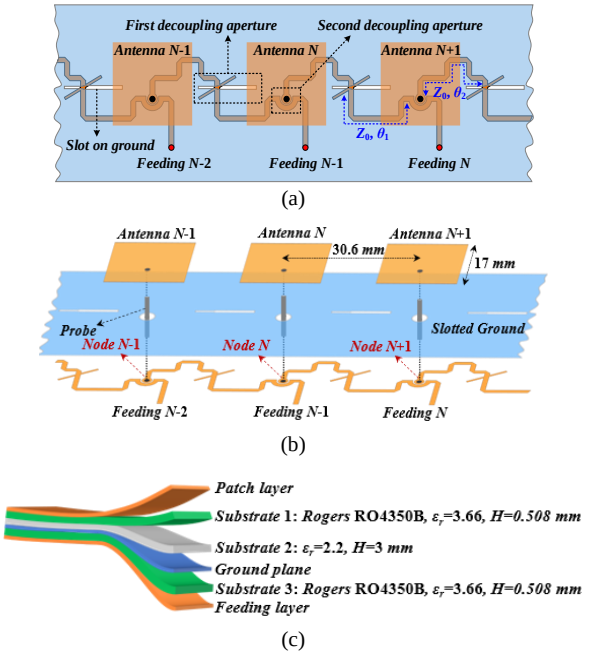

Fig. 1. Configurations of a linear patch antenna array working at 4.9 GHz and integrated with the proposed decoupling structures. (a) Top view. (b) 3-dimension view. (c) Multi-layer description.

would pass through the second and first decoupling apertures successively and reach the feeding probe.

The physical configurations of the decoupling apertures are shown in Fig. 2. As for the first decoupling aperture, a 50-Ω microstrip line is positioned across a slotline resonator etched on the ground plane. Two open-circuited stubs are symmetrically distributed on the microstrip line with respect to the slotline. By changing the relative position (W_1 and H_1) between the slotline and the patch of *Antenna N*, the coupling response between *Node F*1 and *Node N* would be tuned. The second decoupling aperture consists of a 50-Ω microstrip line and a circular pad with a coupling gap, where the pad is connected with the feeding probe of *Antenna N*. The transmission response is determined by the gap dimension (G_1). Normally the values of D_1, D_2, and D_3 are given and non-tunable under the impedance matching condition. A transmission line (Z_0, θ_1) is applied between the first and second decoupling apertures. Between the feeding point of an antenna element and the first decoupling path, a transmission line (Z_0, θ_2) is also inserted. All the electric lengths are referred to the center frequency f_0 = 4.9 GHz in this case. Finally, decoupling resonances at two frequencies f_1 and f_2, would be generated, where $f_1 < f_0 < f_2$.

A. Synthesis and analysis of the proposed decoupling method

A signal flow graph is constructed, as illustrated in Fig. 3, where *Antenna N*-1 and *Antenna N* are selected. Defining that a wave incident at *Node S*1 has a voltage of V_{N-1}, the voltage of the leaking wave at *Node N* would contain three paths, through the second decoupling aperture (*Path* A), the first decoupling aperture (*Path* B), and the coupling path (*Path* C) between patches, correspondingly. Then, the voltages of the three paths can be expressed as

$$V_{N,A} = S_{N,S1} V_{N-1} \tag{1a}$$

$$V_{N,B} = S_{S2,S1} S_{F1,S2} S_{N,F1} V_{N-1} \tag{1b}$$

$$V_{N,C} = S_{S2,S1} S_{F1,S2} S_{F2,F1} S_{N-1,F2} S_{N,N-1} V_{N-1} \tag{1c}$$

where $S_{i,j}$ represents the scattering parameter between *Nodes i* and *j*. The parameter $S_{N,N-1}$ denotes the mutual coupling between the two radiating patches, which can be obtained through full-wave

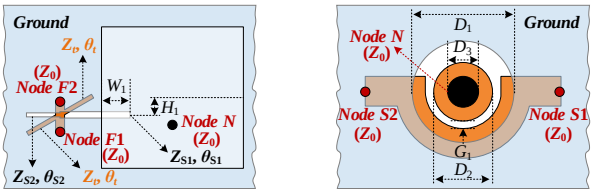

Fig. 2. Configurations of (a) the first and (b) second decoupling apertures.

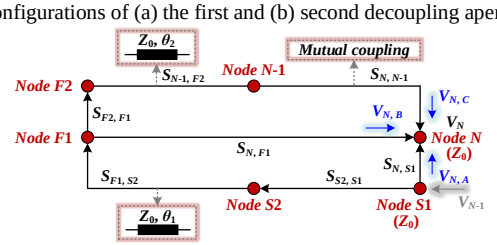

Fig. 3. Signal flow graph of the decoupling between *Antenna N*-1 and *Antenna N*., i.e., between *Node S*1 and *Node N* shown in Fig. 2.

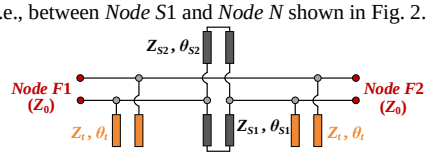

Fig. 4. Equivalent circuit model of the slotline-based lowpass filter.

simulations. Based on transmission line theory, we have that

$$S_{F1,S2} = \cos\theta_1 - j\sin\theta_1 \tag{2a}$$

$$S_{N-1,F2} = \cos\theta_2 - j\sin\theta_2 \tag{2a}$$

As mentioned, the proposed decoupling method could generate two cancellation resonances allocated at the frequencies f_1 and f_2, respectively. At this point, the voltage V_N of the leaking wave at *Node N* should be

$$V_N\big|_{@\, f_1, @\, f_{21}} = \left(V_{N,A} + V_{N,B} + V_{N,C}\right)\Big|_{@\, f_1, @\, f_2} = 0 \tag{3}$$

Substituting (2) into (3), the following relations can be derived under the decoupling condition:

$$\begin{aligned} &S_{N,S1} + S_{S2,S1}(\cos\theta_1 - j\sin\theta_1) \\ &\times\left[S_{N,F1} + S_{F2,F1} S_{N,N-1}(\cos\theta_2 - j\sin\theta_2)\right]\Big|_{@\, f_1, @\, f_2} = 0 \end{aligned} \tag{4}$$

Under the condition derived in (4), a group solution of $S_{N,S1}$, $S_{S2,S1}$, $S_{N,F1}$, $S_{F2,F1}$, θ_1, and θ_2, can be determined theoretically. Next, the first and second decoupling apertures will be studied, respectively.

B. Investigation of the first decoupling aperture

As illustrated in Fig. 2(a), the slotline is utilized to provide the decoupling path between the feeding and the adjacent patch but also applies harmonic suppression. An equivalent circuit of the slotline-based two-port network is established, as shown in Fig. 4. The transmission response of the two-port network can be easily derived. If set that θ_{S1}=90°, θ_{S2}=45°, and θ_t=45°, a lowpass response with harmonic suppression can be achieved, by properly selecting a group value of Z_{S1}, Z_{S2}, and Z_t. Moreover, the harmonic suppression is independent of the characteristic impedance. Fig. 5(a) shows the calculated *S* parameters of the two-port network, with the values of Z_{S1} = 95.3 Ω, Z_{S2} = 54.4 Ω, and Z_t = 77.1 Ω. A three-dimension model with f_0 = 4.9 GHz is also constructures and simulated by using full-wave simulators. The results illustrated in Fig. 5(b) show that a lowpass response is obtained and the first-order harmonic at $2f_0$ is suppressed. By changing the position of the slotline, the coupling (denoting as the 1st decoupling path) between the lowpass filter and *Node N*, i.e., $S_{N,F1}$, can be tuned. As marked in Fig. 2(a), the distances of the slotline departing away from the center of the

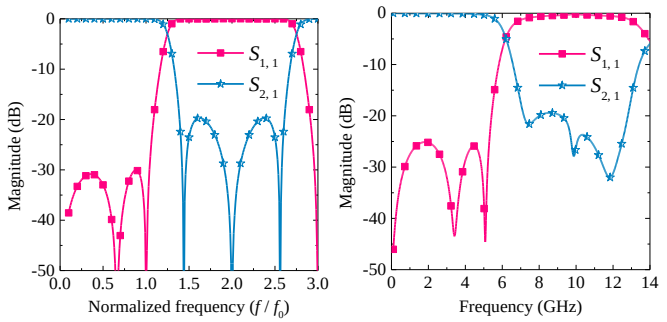

Fig. 5. (a) Calculated *S* parameters of the equivalent circuit shown in Fig. 4. (b) Full-wave simulated *S* parameters of a demonstrator working at 4.9 GHz.

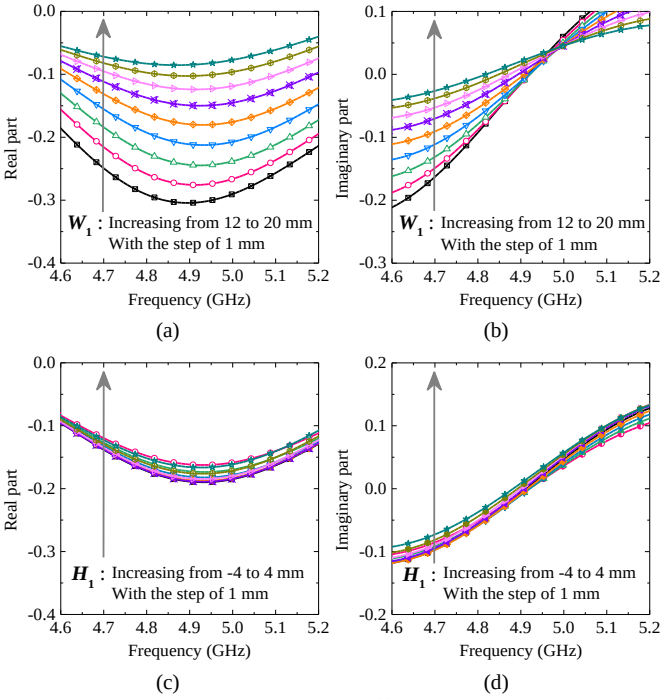

Fig. 6. Full-wave simulated $S_{N,F1}$ against different parameter values. (a) Real and (b) imaginary parts of $S_{N,F1}$ against different W_1, with $H_1 = 0$. (c) Real and (d) imaginary parts of $S_{N,F1}$ against different H_1 with $W_1 = 15$ mm, where the positive direction of H_1 is set as the offset downward from the center of the patch as shown in Fig. 2(a).

radiating patch along vertical and horizontal directions are set as H_1 and W_1, respectively. It is seen from Fig. 6 that by changing the value of W_1, the real and imaginary parts of $S_{N,F1}$ can be adjusted over a wide range. However, the change in the value of H_1 does not bring an obvious change in $S_{N,F1}$. This indicates that the large the value of W_1 is, the small the magnitude of $S_{N,F1}$ would be.

The harmonic suppression performance of the lowpass filter with the patch loading in front is also discussed with different values of W_1 and H_1, as shown in Fig. 7. The results indicate that the lowpass characteristic is not influenced regardless of the values of W_1 and H_1. The harmonics around $2f_0$ (9.8 GHz) are always suppressed. This implies that the harmonic suppression performance would not be affected during decoupling.

C. Study of the second decoupling aperture

As for the second decoupling structure, a graphical study is provided to show the transmission performance between the feeding line and the radiating patch (denoting as the 2nd decoupling path), i.e., $S_{N,S1}$, based on the configuration shown in Fig. 2(b). As discussed, the coupling level of the 2nd decoupling path is mainly

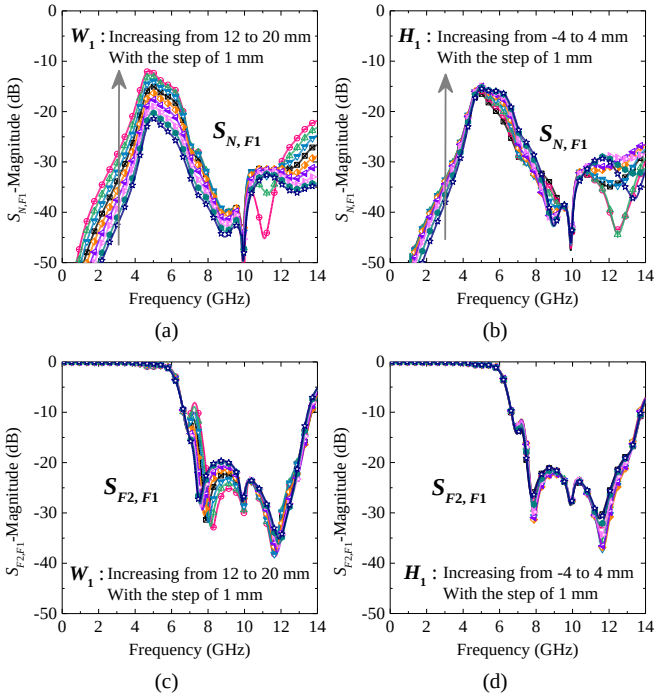

Fig. 7. Full-wave simulated transmission responses of the first decoupling aperture and the leakage to *Node N*.

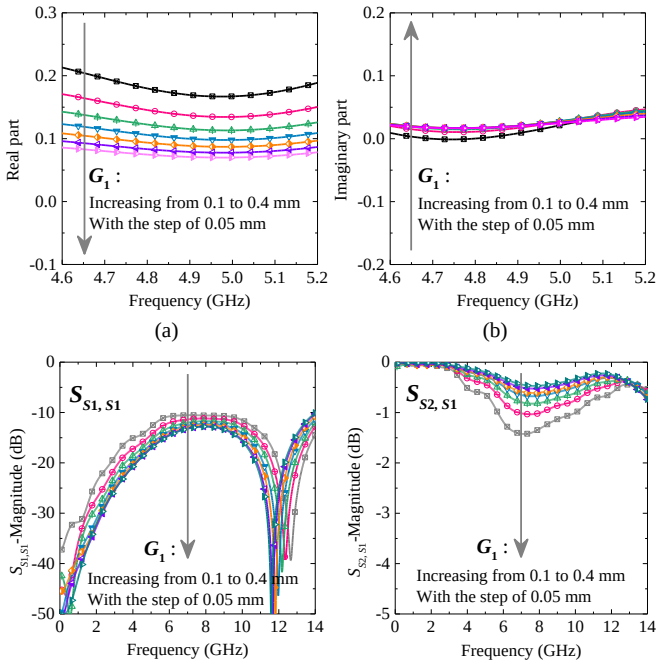

Fig. 8. Simulated $S_{N,S1}$ against different values of G_1 based on Fig. 2. (a) Real and (b) imaginary parts of $S_{N,S1}$. (c) $S_{S1,S1}$ and (d) $S_{N,S1}$.

contributed by the gap size G_1. Here, the values of D_1, D_2, and D_3 are set as 3 mm, 2.4 mm, and 1 mm, correspondingly. Fig. 8 shows the real and imaginary parts of $S_{N,S1}$, against different values of G_1. It is seen that the real part can be tuned among a wide range, while the imaginary part is almost not changed. This denotes that when doing the decoupling operation, the imaginary part of $S_{N,S1}$ can be considered constant. The magnitudes of $S_{S1,S1}$ and $S_{S2,S1}$ against different G_1 are also provided, as shown in Fig. 8(c) and Fig. 8(d), respectively. It is seen that around the operating frequency of 4.9 GHz, *Node S*1 is well-matched. The magnitude of $S_{S1,S1}$ is less than

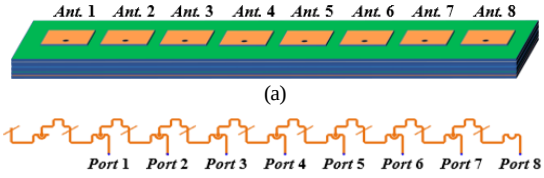

Fig. 9. Configuration of the 1×8 patch antenna array integrated with the proposed decoupling and harmonic suppression structure. (a) 3-dimension view. (b) Decoupling and feeding network with harmonic suppression.

TABLE I
DETERMINED PARAMETER VALUES OF THE DECOUPLED ARRAYS

	f_1 / f_2 (GHz)	W_1 (mm)	H_1 (mm)	G_1 (mm)	θ_1 (º)	θ_2 (º)
Case A	4.6/5.2	14.2	0	0.15	255.8	187.2
Case B	4.7/5.1	15.1	0	0.15	236.2	197.4
Case C	4.8/5.0	14.3	2.3	0.2	204.6	203.5

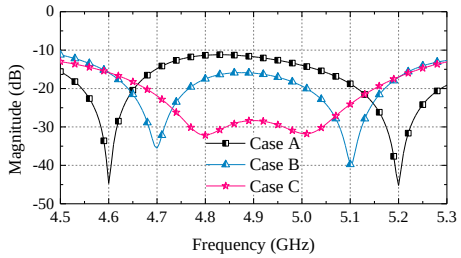

Fig. 10. Calculated mutual coupling levels between *Ports* 4 and 5 of the decoupled antenna arrays with different settings of decoupling resonances.

–10 dB among the studied frequency band. These results imply that the lowpass and harmonic-suppression responses would not be influenced when the first and second decoupling apertures are cascaded to establish a dual-resonance decoupling network.

III. DESIGN EXAMPLE

A design procedure is summarized to provide an overview of the parameter determinations, described as follows.

***Step 1*:** Determining the values of Z_{S1}, Z_{S2}, Z_t, θ_{S1}, θ_{S2}, and θ_t, to construct the lowpass filter, based on the model given in Fig. 4.

***Step 2*:** Selecting the two decoupling frequencies f_1 and f_2.

***Step 3*:** Extracting the coupling response between the lowpass filter and the adjacent radiating patch through the slotline, based on the graphical study given in Fig. 6 and Fig. 7.

***Step 4*:** Extracting the coupling response between the second decoupling aperture and the feeding point of the adjacent radiating patch, based on the graphical study illustrated in Fig. 8.

***Step 5*:** Constructing the signal flow graph.

***Step 6*:** Determining the values of $S_{N,S1}$, $S_{S2,S1}$, $S_{N,F1}$, $S_{F2,F1}$, θ_1, and θ_2, under the condition expressed in (4) for decoupling purposes. Finding the values of W_1, H_1 and G_1 corresponding to the obtained transmission responses of $S_{N,S1}$, $S_{S2,S1}$, $S_{N,F1}$, and $S_{F2,F1}$.

***Step 7*:** Determining the physical layout of the network for the given antenna array through full-wave simulations.

Then, a design example of a 1×8 patch antenna array working at 4.9 GHz integrated with the proposed decoupling structure is developed, as shown in Fig. 9. Since the two decoupling resonances are allocated at the two sides of the center frequency, the decoupling bandwidth should be mainly determined by the two decoupling resonances. Table I lists the obtained parameter values of three cases with different values of f_1/f_2. The calculated results of the 1×8 array under the setting of three cases are given in Fig. 10, where the coupling between *Ports* 4 and 5 is selected as the representative one. It is verified that the farther the two decoupling frequencies are, the higher the coupling level at the center frequency would be. In this section, the setting of Case C is selected as the one to be further fabricated and measured.

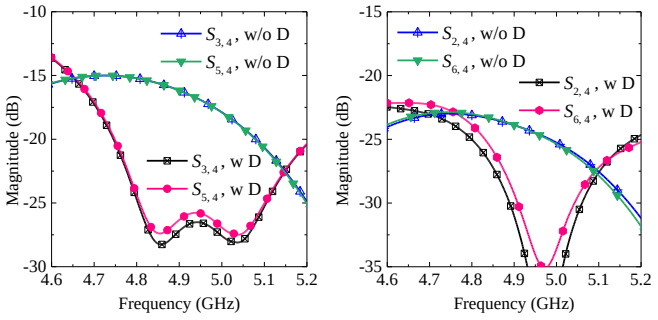

Fig. 11. Simulated *S* parameters of decoupled and coupled antenna arrays. (a) $S_{3,4}$ and $S_{5,4}$. (b) $S_{2,4}$ and $S_{6,4}$, where "w/o D" denotes without decoupling.

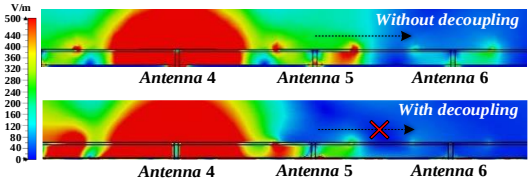

Fig. 12. Simulated electric-field distribution of the area close to the array without and with decoupling when *Port* 4 is excited.

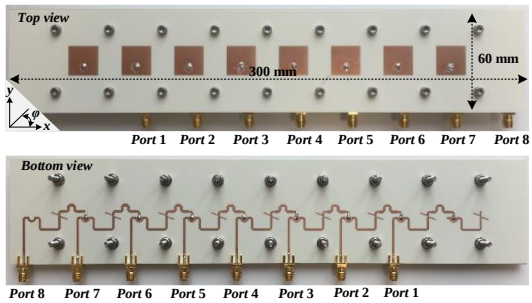

Fig. 13. Photos of the fabricated demonstrator.

Fig. 11 illustrates the simulated coupling levels of the decoupled 1×8 patch antenna array. The leakage between adjacent elements of the decoupled array is suppressed to less than –25 dB as expected. Moreover, despite no direct decoupling operation, the mutual coupling paths between non-adjacent elements are canceled, i.e., $S_{2,4}$ and $S_{6,4}$ as shown in Fig. 11(b). This is also contributed by the adjacent-element decoupling. Fig. 12 plots the near-field electrical field distribution when *Port* 4 is excited. It is seen that the EM waves propagating from the excited patch to non-adjacent patches are suppressed, leading to an improved non-adjacent isolation level.

IV. MEASUREMENT AND DISCUSSION

The developed example of the 1×8 decoupled antenna array is fabricated and assembled, as shown in Fig. 13. Note that the decoupling structures are also integrated with the elements at the two edges, i.e., elements 1 and 8, to make sure that the feeding of all the elements are identical. The measured *S* parameters of the decoupled array are shown in Fig. 14, where *Port* 4 is chosen as the representative port. The result in Fig. 14(a) denotes that the impedance matching response is improved after being integrated with the proposed decoupling method. The impedance bandwidth is extended from 400 MHz (4.7 to 5.1 GHz) to over 900 MHz after decoupling (4.3 to 5.2 GHz), referred to $|S_{i,i}| \leq -10$ dB, denoting a fractional bandwidth of 18.9%. The coupling paths between adjacent elements, i.e., $S_{3,4}$ and $S_{5,4}$, are suppressed from –15 dB to less than –25 dB. The coupling among non-adjacent elements is also suppressed, as shown in Figs. 14(d), 14(e), and 14(f).

Note that the coupling between *Ports* 4 and 7 of the decoupled antenna array is suppressed around the center frequency, at the cost of slight improvement of the coupling level when the frequency

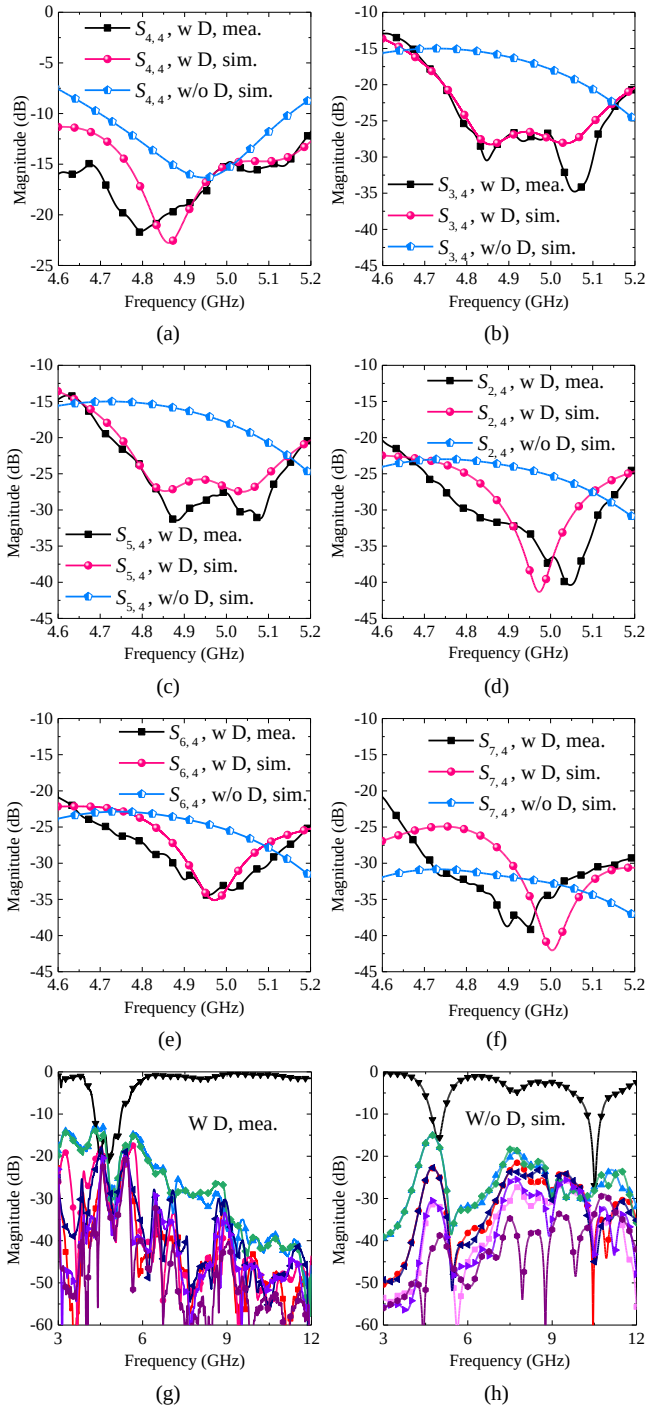

Fig. 14. Measured and simulated *S* parameters of the decoupled antenna array when *Port* 4 is excited. (a) $S_{4,4}$. (b) $S_{3,4}$. (c) $S_{5,4}$. (d) $S_{2,4}$. (e) $S_{6,4}$. (f) $S_{7,4}$. (g) Out-of-band suppression (g) with and (h) without decoupling.

departs away from the center frequency, as shown in Fig. 14(f). Despite this, the coupling level is still kept at a low level. In a word, an isolation level of higher than 25 dB is achieved within the range from 4.8 to 5.1 GHz, indicating a fractional bandwidth of 6.1%. The out-of-band responses are shown in Figs. 14(g) and 14(h). It is seen that the harmonic up to 12 GHz is well suppressed. Notice that the coupling responses of the edge elements and other elements would have slight difference, due to the different EM boundaries. Despite this, the decoupling performance of the edge elements still features expected responses, which is not detailed for brevity.

The radiation patterns of the embedded element at 4.9 GHz given

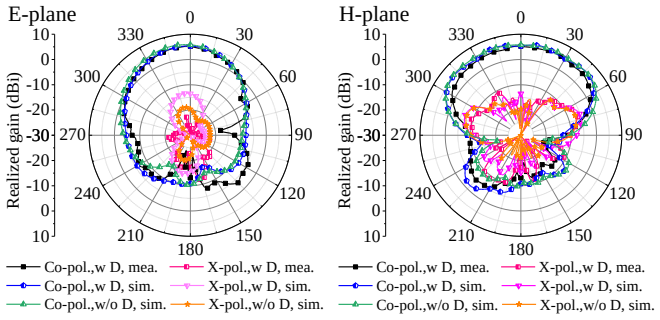

Fig. 15. Measured and simulated radiation patterns when *Port* 4 is excited. (a) E-plane and (b) H-plane.

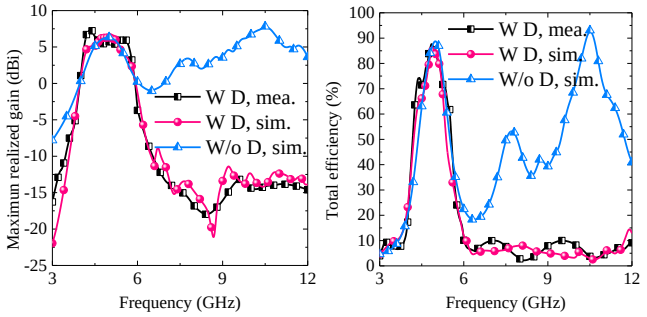

Fig. 16. Measured and simulated (a) realized gain and (b) total efficiency, when *Port 4* is excited.

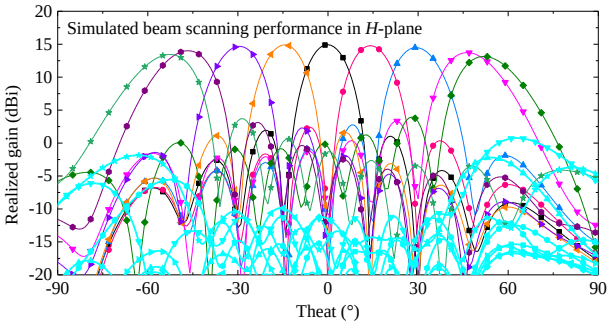

Fig. 17. Calculated beam-scanning performance of the decoupled array in *H*-plane at 4.9 GHz, where the cyan curves are the cross-polarization patterns.

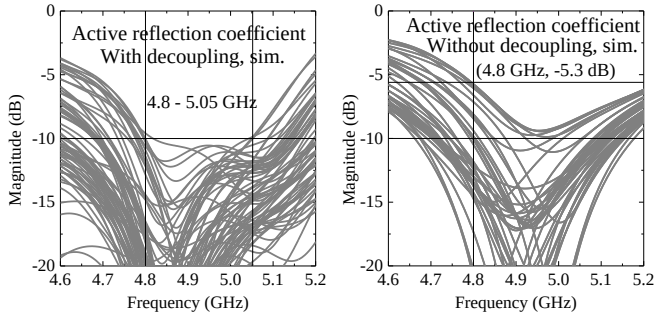

Fig. 18. Calculated active reflection coefficients of all the ports of the array (a) with and (b) without decoupling under the beam scanning range of ±53° at 4.9 GHz.

in Fig. 15 verify that the decoupling method does not affect the radiating of the antenna elements. The maximum realized gain and total efficiency of the decoupled array when *Port* 4 is excited, are illustrated in Fig. 16(a) and Fig. 16(b), respectively. The gain at the harmonic frequency is reduced from 7.8 dBi to lower than –12 dBi. The peak total efficiency is around 86%, and the in-band (4.8-5.1 GHz) total

TABLE II
COMPARISON BETWEEN SOME PUBLISHED FEEDING-BASED DECOUPLING METHODS AND THE PROPOSED SCHEME

Ref./Year	Array configuration	Element distance	Fractional decoupling bandwidth	In-band total efficiency	Insertion loss (dB)	Harmonic suppression
[12]/2020	1×2 / H-coupled, @2.0 GHz	$0.1\lambda_0$	23.7% (≤ –20 dB)	≥ 73.9%	≈ 0.5	/
	1×3 / Triangular, @2.4 GHz	$0.14\lambda_0$	9.6% (≤ –20 dB)	/	/	/
[13]/2019	1×5 / E-coupled, @5.55 GHz	$0.45\lambda_0$	1.1% (≤ –20 dB)	/	/	/
	1×3 / H-coupled, @5.5 GHz*	$0.48\lambda_0$	4.5% (≤ –15 dB)	/	/	/
[14]/2019	4×4, @4.9 GHz*	$0.5\lambda_0$	2% (≤ –25 dB)	≥ 70%	0.45	/
[15]/2021	1×8 / H-coupled, @4.9 GHz	$0.5\lambda_0$	2% (≤ –25 dB)	≥ 80%	≈ 0	/
	4×4, @4.9 GHz	$0.5\lambda_0$@E-plane $0.6\lambda_0$@H-plane	7% (≤ –24.7 dB)	≥ 70.9%	0.6	/
This work	1×8 / H-coupled, @4.9 GHz	$0.5\lambda_0$	6.1% (≤ –25 dB)	≥ 80%	≈ 0	Yes

* denotes the full-wave simulated results, and / represents Not Given.

efficiency after decoupling is higher than 80%, with nearly no additional insertion loss compared to the coupled array.

V. BEAM SCANNING AND PERFORMANCE COMPARISON

Beam-scanning performance of the decoupled antenna array is discussed by using full-wave simulations. The maximum radiation is oriented in the directions of 0º, ±15º, ±30º, ±45º, and ±53º at H-plane (φ=0 º), as illustrated in Fig. 17. The peak gain is with a small drop from 14.9 to 13.4 dBi during beam scanning. The calculated active reflection coefficients of all ports of the decoupled array among the beam-scanning range of ±53º are shown in Fig. 18(a). The worst active reflection coefficient within the band of 4.8 to 5.05 GHz is almost less than –10 dB, while the one of the coupled array is higher than –5.3 dB. The common band of the active impedance matching, and the decoupling bandwidths almost overlap with each other, indicating that the proposed scheme makes the array working stable.

To show the advantages of the proposed method, some recently published antenna decoupling methods operating at the feeding layer are summarized, as listed in Table II. Note that in this work, an H-plane coupled array is selected as the design example. Considering the decoupling principle, the proposed scheme is also effective for E-plane coupled arrays. As discussed, the decoupling bandwidth is normally narrow due to the strong resonance of microstrip lines. The work reported in [15] achieved a decoupling bandwidth of 7%, at the cost of a large element distance of $0.6\lambda_0$ and a decreased total efficiency. The proposed decoupling uses two decoupling resonances to extend bandwidth, without introducing additional insertion loss. Besides, harmonic suppression is achieved by sharing the decoupling structure.

VI. CONCLUSION

A simple and compact decoupling scheme featuring dual-resonance and harmonic suppression is proposed and investigated in this communication for patch antenna arrays. The performance of the proposed method has been verified by theoretical, full-wave simulated, and measured results. The coupling suppression between adjacent and non-adjacent elements is demonstrated, and the beam scanning performance is also discussed as well. These make the proposed method valuable and attractive for large-scale antenna arrays to future wireless communication applications.

REFERENCES

[1] T. L. Marzetta, "Massive MIMO: An Introduction," *Bell Labs Technical Journal*, vol. 20, pp. 11-22, 2015.

[2] A. Elsakka et al., "A MM-Wave Phased-Array Fed Torus Reflector Antenna With ±30° Scan Range for Massive-MIMO Base-Station Applications," *IEEE Transactions on Antennas and Propagation*, vol. 70, no. 5, pp. 3398-3410, May 2022.

[3] M. Temiz, E. Alsusa, L. Danoon and Y. Zhang, "On the Impact of Antenna Array Geometry on Indoor Wideband Massive MIMO Networks," *IEEE Transactions on Antennas and Propagation*, vol. 69, no. 1, pp. 406-416, Jan. 2021.

[4] R. Janaswamy, "Effect of Element Mutual Coupling on The Capacity of Fixed Length Linear Arrays," *IEEE Antennas and Wireless Propagation Letters*, vol. 1, pp. 157-160, 2002.

[5] L. Savy and M. Lesturgie, "Coupling Effects in MIMO Phased Array," *2016 IEEE Radar Conference (RadarConf)*, Philadelphia, PA, USA, 2016, pp. 1-6.

[6] B. Wang, Y. Chang and Y. Sun, "Performance of the Large-Scale Adaptive Array Antennas in the Presence of Mutual Coupling," *IEEE Transactions on Antennas and Propagation*, vol. 64, no. 6, pp. 2236-2245, June 2016.

[7] B. Liu, X. Chen, J. Tang, A. Zhang and A. A. Kishk, "Co- and Cross-Polarization Decoupling Structure With Polarization Rotation Property Between Linearly Polarized Dipole Antennas With Application to Decoupling of Circularly Polarized Antennas," *IEEE Transactions on Antennas and Propagation*, vol. 70, no. 1, pp. 702-707, Jan. 2022.

[8] K. -L. Wu, C. Wei, X. Mei and Z. -Y. Zhang, "Array-Antenna Decoupling Surface," *IEEE Transactions on Antennas and Propagation*, vol. 65, no. 12, pp. 6728-6738, Dec. 2017.

[9] M. Li, B. G. Zhong and S. W. Cheung, "Isolation Enhancement for MIMO Patch Antennas Using Near-Field Resonators as Coupling-Mode Transducers," *IEEE Transactions on Antennas and Propagation*, vol. 67, no. 2, pp. 755-764, Feb. 2019.

[10] A. A. Diman et al., "Efficient SIW-Feed Network Suppressing Mutual Coupling of Slot Antenna Array," *IEEE Transactions on Antennas and Propagation*, vol. 69, no. 9, pp. 6058-6063, Sept. 2021.

[11] J. Kornprobst et al., "Compact Uniform Circular Quarter-Wavelength Monopole Antenna Arrays With Wideband Decoupling and Matching Networks," *IEEE Transactions on Antennas and Propagation*, vol. 69, no. 2, pp. 769-783, Feb. 2021.

[12] M. Li, L. Jiang, and K. L. Yeung, "A Novel Wideband Decoupling Network for Two Antennas Based on the Wilkinson Power Divider," *IEEE Transactions on Antennas and Propagation*, vol. 68, no. 7, pp. 5082-5094, July 2020.

[13] X. -J. Zou, G. -M. Wang, Y. -W. Wang and H. -P. Li, "An Efficient Decoupling Network Between Feeding Points for Multielement Linear Arrays," *IEEE Transactions on Antennas and Propagation*, vol. 67, no. 5, pp. 3101-3108, May 2019.

[14] Y. -M. Zhang, S. Zhang, J. -L. Li and G. F. Pedersen, "A Transmission-Line-Based Decoupling Method for MIMO Antenna Arrays," *IEEE Transactions on Antennas and Propagation*, vol. 67, no. 5, pp. 3117-3131, May 2019.

[15] Y. -M. Zhang and S. Zhang, "A Novel Aperture-Loaded Decoupling Concept for Patch Antenna Arrays," *IEEE Transactions on Microwave Theory and Techniques*, vol. 69, no. 9, pp. 4272-4283, Sept. 2021.

[16] M. Li, S. Tian, M. -C. Tang and L. Zhu, "A Compact Low-Profile Hybrid-Mode Patch Antenna With Intrinsically Combined Self-Decoupling and Filtering Properties," *IEEE Transactions on Antennas and Propagation*, vol. 70, no. 2, pp. 1511-1516, Feb. 2022.

[17] Y. -M. Zhang, Q. -C. Ye, G. F. Pedersen and S. Zhang, "A Simple Decoupling Network With Filtering Response for Patch Antenna Arrays," *IEEE Transactions on Antennas and Propagation*, vol. 69, no. 11, pp. 7427-7439, Nov. 2021.